

Design of the extreme AO system for SPHERE, the planet-finder instrument of the VLT

T. Fusco^a, C. Petit^a, G. Rousset^{b,a}, J.-F. Sauvage^a, K. Dohlen^c, D. Mouillet^d, J. Charton^d, P. Baudoz^b, M. Kasper^e, E. Fedrigo^e, P. Rabou^d, P. Feautrier^d, M. Downing^e, P. Gigan^b, J.-M. Conan^a, J.-L. Beuzit^d, N. Hubin^e, F. Wildi^f, P. Puget^b

^aONERA, BP 72, 92322 Chatillon France,

^bLESIA, Observatoire de Paris, 5 Place Jules Janssen 92195 Meudon, France,

^cLAM, Observatoire de Marseille, BP 8, F-13376 Marseille, France,

^dLAOG, Observatoire de Grenoble, BP 53, F-38041 Grenoble, France,

^eESO, Karl-Schwarzschild-StraÙe 2, Garching, D-85748 Germany,

^fHES-SO, 1, rte de Cheseaux CH-1401 Yverdon

ABSTRACT

The SPHERE system aims at the detection of extremely faint sources (giant extra-solar planet) in the vicinity of bright stars. Such a challenging goal automatically requires the use of a coronagraphic device to cancel out the flux coming from the star and smart imaging technics which have to be added to reach the required contrast for exo-planet detection (typically 10^{-6} - 10^{-7} in contrast). In this frame of the SPHERE project a global system study has demonstrated the feasibility of an AO system for the direct exoplanets detection.

A detailed description of this system is proposed in this paper. The main trade-offs are discussed and justified and all the subsystems briefly presented. The realization phase has begun in 2006 and we foresee to obtain a first light at the VLT in 2010.

Keywords: high angular resolution, adaptive optics

1. INTRODUCTION

We present here the results of the phase A study of the adaptive optics system for the SPHERE instrument (¹). The main scientific objective of SPHERE is the direct detection of photons coming from giant extrasolar planets (between 1 and 20 Jupiter masses). Any detection will then be followed by a first characterization of the planet atmosphere (clouds, dust content, methane, water absorption...). In addition, the survey of an extended number of stars (typically a few hundreds) is mandatory in order to perform meaningful statistical studies. Such extremely challenging scientific objectives directly translate into a relatively complex high contrast instrument. Coronagraphic and smart imaging (differential imaging for instance) capabilities are essential to reach the high contrast (close to the optical axis) required for direct extrasolar planet detection. From the ground, the core of any high contrast instrument is an extreme adaptive optics (XAO) system correcting for the perturbation induced by the atmospheric turbulence as well as for the internal aberrations of the instrument itself.

Based on the specifications provided by the astronomers (²) and on the constraints of the high contrast instrumentation, the XAO must fulfill the following three high level requirements: 1) ensure the measurement and correction of the turbulent phase perturbations, of the telescope and system common optics aberrations, of the non-common path aberrations (main AO loop); 2) ensure an extremely high stability (at low temporal frequency) of the optical axis at the level of the coronagraphic mask (Auxiliary Sensor [AS]); 3) ensure the measurement and the correction of any pupil motion (Pupil Motion Sensor [PMS]). In the following sections, we will mainly focus on the main AO loop design. The two other requirements (essential to ensure optimal coronagraphic extinction and, *in fine*, planet detection performance) will only be briefly addressed.

Further author information: (Send correspondence to T.F.)

T.F: E-mail: thierry.fusco@onera.fr, Telephone: +33 (0)1 46 73 47 37

2. AO LOOP PERFORMANCE IN THE FOCAL PLANE

The SPHERE system aims at the detection of extremely faint sources (giant extrasolar planets) in the vicinity of bright stars. Such a challenging goal requires the use of a coronagraphic device to cancel out the flux coming from the star itself. Even if additional smart imaging techniques are added to reach the required contrast for extrasolar planet detection (typically 10^{-6} - 10^{-7} in contrast), the coronagraphic image is a basis for the AO optimization. Moreover, unlike classical AO systems, residual variance or Strehl ratio are not sufficient anymore to optimize the system and to derive the pertinent trade-offs. They have to be replaced by a more accurate parameter which can provide information on the coronagraphic image shape in the focal plane. The purpose of the coronagraph is to remove the coherent light coming from the on-axis guide star (GS). Therefore one can analytically define a "perfect coronagraph" using the following equations:

$$I_{corona}(\rho) = \left\langle \left| \text{FT} \left[P(r)A(r)e^{i\varphi_{res}(r)} - \sqrt{\exp[-\sigma_{\varphi+\log(A)}^2]} P(r) \right] \right|^2 \right\rangle \quad (1)$$

where $\langle \cdot \rangle$ stands for a statistical average and with $A(r)$ the wavefront amplitude, $\varphi_{res}(r)$ the residual phase after AO correction, $P(r)$ the pupil function and $\sigma_{\varphi+\log(A)}^2$ the residual variance gathering phase and log-amplitude effects. When only a partial correction is performed, the coherent peak is removed and only the incoherent light (the residual uncorrected speckles) remains. In that case, it is easy to show that, as a first approximation (first order expansion) the coronagraphic image is proportional to the residual phase power spectral density.

3. BALANCE OF AN ERROR BUDGET

The whole AO study is based on the balance of an error budget. A first approximation (first order expansion) of this coronagraphic shape is given by the residual phase power spectral density (PSD) as shown in Section 2. Therefore, the global error budget for the AO system can be summarized as follow:

$$\begin{aligned} \text{PSD}_{res} = & \underbrace{\text{PSD}_{scint} + \text{PSD}_{diff} + \text{PSD}_{refrac} + \text{PSD}_{aniso}}_{\text{atmospheric limitation}} \\ & + \underbrace{\text{PSD}_{fit} + \text{PSD}_{temp} + \text{PSD}_{alias} + \text{PSD}_{noise}}_{\text{low order residual error}} + \underbrace{\text{PSD}_{calib} + \text{PSD}_{aberr}}_{\text{calibration errors}} \end{aligned} \quad (2)$$

AO loop residual error

A complete description can be found in.³ PSD_{res} is expressed in terms of residual variance per spatial frequency in order to highlight the range of spatial frequencies which is affected by each error item. The optimization of this error budget will be performed, keeping in mind three main criteria:

- The corrected area, i.e. the focal plane area where the image contrast is significantly improved by the AO system. It mainly drives the choice of the number of actuators (the correction area is equal to λ_{im}/d in diameter, where d is the actuator spacing). Considering the typical targets which will be observed by SPHERE and the imaging wavelengths (J, H and K bands), this area has to be larger than 0.8 arcsec in diameter.
- The detectivity level, i.e. the capability of the whole system to detect the planet signal. This level is affected by the AO loop errors (temporal, noise, aliasing...) which evolve rapidly with time and can be calibrated using differential imaging and a reference PSF. It can also be degraded by the telescope and the system high spatial frequencies and non-common path aberrations which slowly evolve with time and represent the ultimate limitation for the differential imaging and reference PSF subtraction techniques. The minimization of the slowly variable defects implies the measurement and the correction of non-common path aberrations (see Section 6) as well as the stabilization of the optical beam during a whole observation sequence (see Section 7.2).

- The system sensitivity. This criterion is driven by the number of stars to be observed but highly depends on the detectivity level and the corrected area size. Indeed, the larger the corrected area the smaller the available flux per individual measurement zones (sub-aperture in the case of a SH device for instance). In addition, increasing the detectivity level implies a reduction in terms of temporal and noise errors, which leads to a faster system working on brighter guide stars for wavefront sensing. A first trade-off between scientific goals and system requirements has led to a limiting magnitude of 8 in H-band (corresponding to magnitudes 10-11 for visible band, depending on the GS types) for the system, implying that the detectivity capabilities have to remain optimum up to this magnitude.

In addition to this three scientific criteria, other constraints have to be taken into account during the instrument design: 1) use of well-proven technologies if possible; 2) new developments for critical issues only, with associated experimental validations; 3) the system has to be built on a tight schedule (5 years typically) with finite manpower and budget. These last three points are essential to minimize the risk factor during the instrument realization.

4. ATMOSPHERIC LIMITATIONS

The atmospheric limitations ⁽⁴⁾ which gather all the errors due to propagation effects (scintillation, diffraction, anisoplanatism and differential refraction effects). Full correction of scintillation effects would only lead to an equivalent reduction of the phase variance smaller than 20 nm rms. In comparison of the small gain in performance, the system complexity is highly increased (two DM, measurement device, reconstruction process...). Considering the small expected gain, even if the scintillation is fully corrected (which is far from being obvious) it has been decided not to consider a scintillation corrector for the VLT Planet Finder instrument.

5. AO LOOP RESIDUAL ERRORS

The AO loop residual errors which gather all the “classical” AO loop errors and can be sub-divided in two main parts described in the following sub-sections.

5.1. The fitting error

The fitting errors (high order modes not corrected by AO, i.e. frequencies higher than the AO spatial cut-off frequency). Considering the Planet Finder Top Level Specifications, the minimization of the global error budget is not the only pertinent criterion, the spatial repartition of the errors has also to be taken into account. In particular, the detectivity performance is also linked to the capacity of the AO system to “clean up the PSF” (i.e. to be as close as possible to the diffraction pattern) in an area of more than 0.75” in radius from the optical axis. This corrected area (Corr) in the focal plane is directly linked to the inter-actuator distance ($d = D/(n_{act} - 1)$, where n_{act} is the linear number of actuators in the telescope diameter D) with the following relation: $corr = \lambda_{im}/2d$. Decreasing d , that is increasing the number of actuators, has however consequences in term of the system limiting magnitude. Indeed, the larger the number of DM actuators, the larger the number of WFS sub-apertures and hence the smaller the number of available photons per sub-aperture and per frame.

All these requirements have been translated into technical specifications for a Tip-Tilt and Deformable mirror. The realization phase of the DM (by the CILAS cpngie) has begun in 2005 for a final product available in mid-2007. The main characteristics of this DM are listed below:

- 41x41 actuators (1377 valid actuators)
- inter-actuator distance 4.514x4.5 mm (to deal with the beam angle in the optical path)
- maximum stroke ± 3.5 (goal 4.1) μm mechanical. The first results on a mock up developed by CILAS show that this specification is already achieved with some margins (a $\pm 5\mu m$ has been measured)
- inter-actuator stroke $\pm 1.2\mu m$ (goal 1.5). Again, mock-up results show a larger stroke ($\pm 2\mu m$).
- Coupling factor: 20 (goal 30 %). Mock up result is well within this range.

- Settling time $\leq 300\mu\text{s}$ for an overshoot $\leq 80\%$
- Hysteris lower than 5 % (goal 3 %)
- best flat $\leq 10\mu\text{m}$ mechanical (goal 5) rms

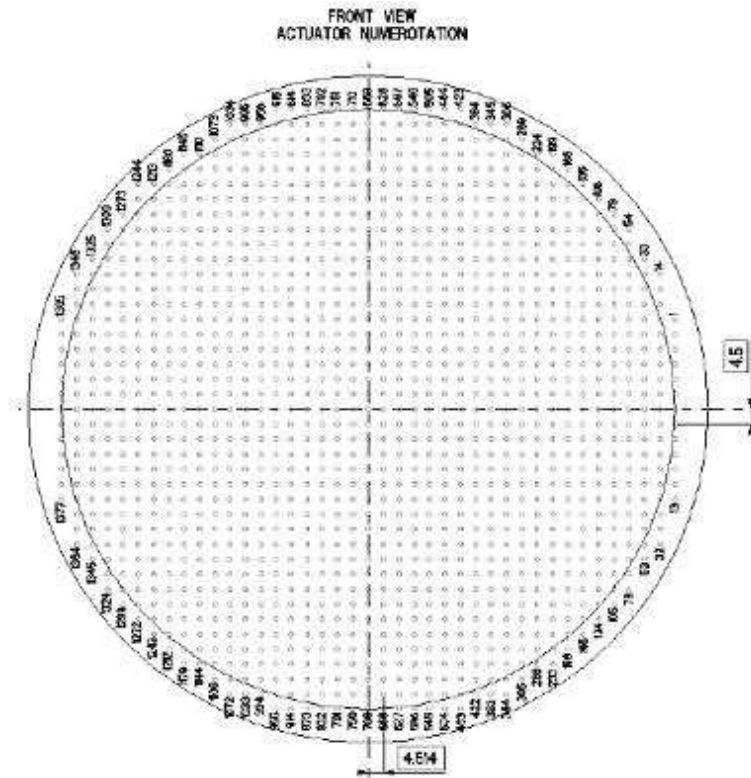


Figure 1: HODM actuators view (1377 useful actuators)

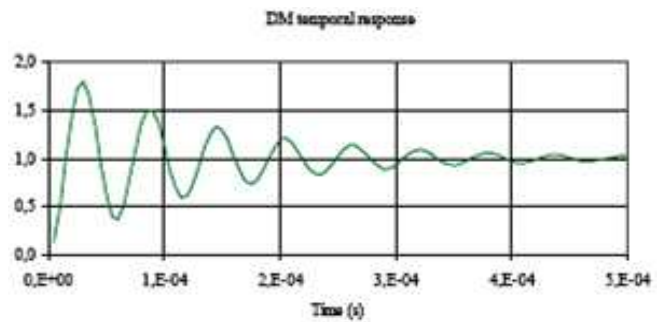
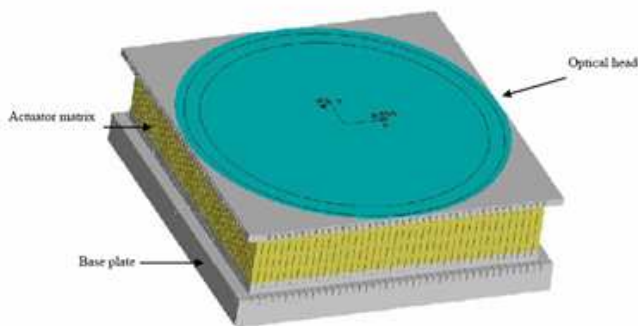


Figure 1. [up] Actuator geometry wrt the telescope pupil 41x41 actuators with 1377 valid). [Down] A 3D representation of the DM and a simulation of its settling time (for one actuator).

The figure 1 shows the actuator geometry, a 3D view of the DM and a simulation (made by CILAS) of its settling time.

The TTM is under Observatoire de Meudon responsibility. Its main characteristics are

- a amplitude of ± 2.5 arcseconds on sky
- a resolution ≤ 0.5 mas on sky
- a bandwidth (-3db) larger than 1 kHz

5.2. The errors on AO corrected modes

These errors gather the aliasing, temporal and noise effects and affect the low order modes that is the inner part of the image.

- i Aliasing error: these effects are due to high spatial frequencies seen as low ones by the WFS device. The aliasing error is directly linked to the fitting error and in the specific case of SH WFS it corresponds to roughly 40% of the total fitting error variance. It dramatically increases the PSF residuals in its corrected area. A concept has been recently proposed ⁽⁵⁾ to significantly reduce the aliasing effect. This device has been deeply studied and optimized with respect to the system and turbulence characteristics (spectral bandwidth, WFS sampling, turbulence ...). In addition, an experimental validation of the concept has been conducted using the ONERA AO bench (see⁶), in closed loop and with turbulence. A gain brought by a filtering device has been clearly demonstrated and it has been shown that the experimental results are in good agreement with the simulation, which validates the potentiality of the concept and its use in the SPHERE design.

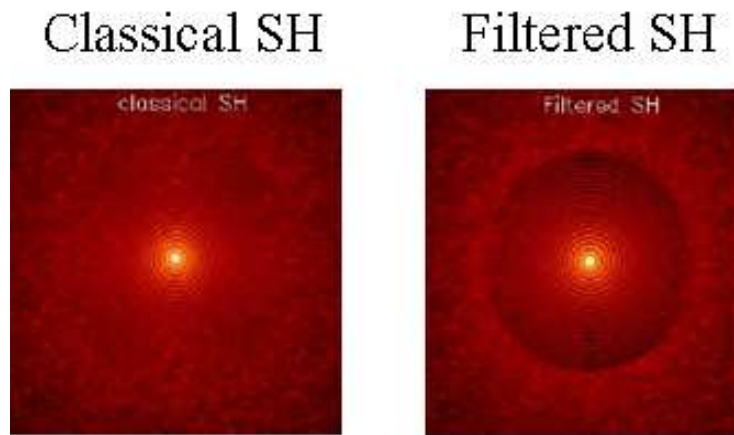


Figure 2. Effect of the filtered SH concept on corrected image. [Left] PSF obtained with a classical SH, [Right] PSF obtained with a filtered one.

- ii Temporal error: the AO loop temporal behavior depends on each AO components (detector integration time, readout noise, real-time computations of commands from WFS data, numerical corrector, digital-analog converter, high voltage amplifier, DM actuator temporal response) and turbulence characteristics. The optimal way to deal with all these parameters is to design a Kalman filter based control algorithm ⁽⁷⁾. An example of the gain brought by the Kalman filter is highlight on Figure 3 Nevertheless, practical implementation of such a control law is complex and requires more computing power, especially for high order systems. This leads to a significant increase of the RTC complexity. A hybrid solution has been considered to deal with this problem. An optimal modal gain integrator has been chosen to control high order modes while a Kalman filter has to be considered for tip-tilt modes to optimally correct turbulence and vibration effects. Even with this trade-off, RTC remains a extremely challenging component. The large number of degree of freedom leads to a complex design. A complete analysis of the loop delays and

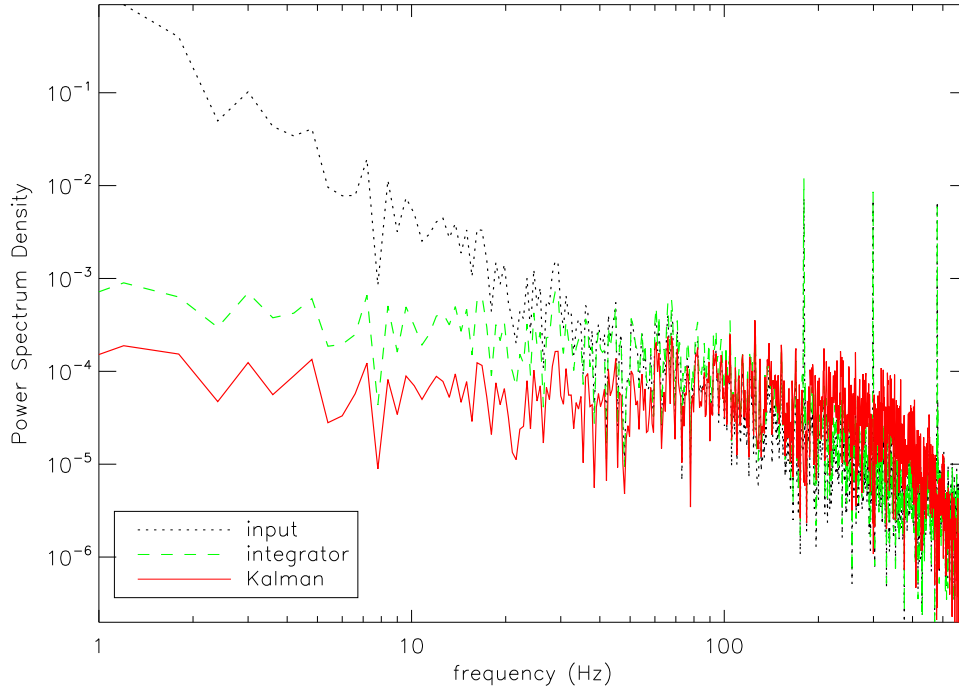


Figure 3. Gain brought by a Kalman filter on the Tip-Tilt correction. In black - dotted line, the un-corrected tip-tilt power spectral density [PSD] (turbulence and 3 vibration pattern located after the AO system bandwidth). In green-dashed line, the residual PSD for a classical integrator (vibrations are not corrected and even slightly amplified). In red-solid line, the results obtained using a Kalman filter. The turbulent part is better corrected (due to the predictive part of the filter) and, more important, the vibration are completely corrected.

system performance has shown that the total latency of the RTC (that is the delay allocated to voltages computation between the last CCD pixel read-out and the last computed voltages) has to be smaller than $120 \mu s$ (goal 80), assuming a 1.2 kHz read-out frequency of the CCD. The RTC will be developed at ESO and based on the SPARTA platform.

iii WFS measurement error: a comparison between SH and Pyramid WFS in the frame of the SPHERE AO system has been performed. In both cases, performance, required calibrations and optimizations, as well as fundamental limitations have been identified and quantified. From the WFS performance, stability, complexity and risk evaluation, a spatially filtered SH WFS, combined with a new optimized slope estimation algorithm ⁽⁸⁾, has been chosen as a baseline for the SPHERE AO system. The system sensitivity is a critical issue for the SPHERE system. In order to increase the limit magnitude of the AO system, the choice of a EMCCD has been done. This challenging device has to combine a high sampling frequency (1.2 kHz) with a small read-out noise. The main characteristics of the CCD are listed hereafter:

- spectral range: from 0.45 to 0.9 μm
- 540x540 pixels
- read-out noise (including the controller) lower than 1 e-
- read-out frequency larger than 1.2 kHz

The chip will be developed by E2V and the controller will be developed at ESO. The final WFS camera should allow us to reach a limiting magnitude of around 10-11 (depending on GS type ⁽⁹⁾).

6. CALIBRATION ERRORS

The calibration errors⁽¹⁰⁾ that gather the AO loop mis-calibration (interaction matrix and reference slopes) and the mis-calibration of the non-common path aberrations (NCPA). Effects of mis-alignment on system performance have been studied leading to tight specifications on system stability (pupil conjugaison between DM and WFS, pupil motion ...). NCPA will be measured using a phase diversity approach¹¹ and corrected in closed loop through a modification of the WFS references. The concepts of the NCPA pre-compensation as well as experimental results obtained with the ONERA AO bench are shown in the figure 4.

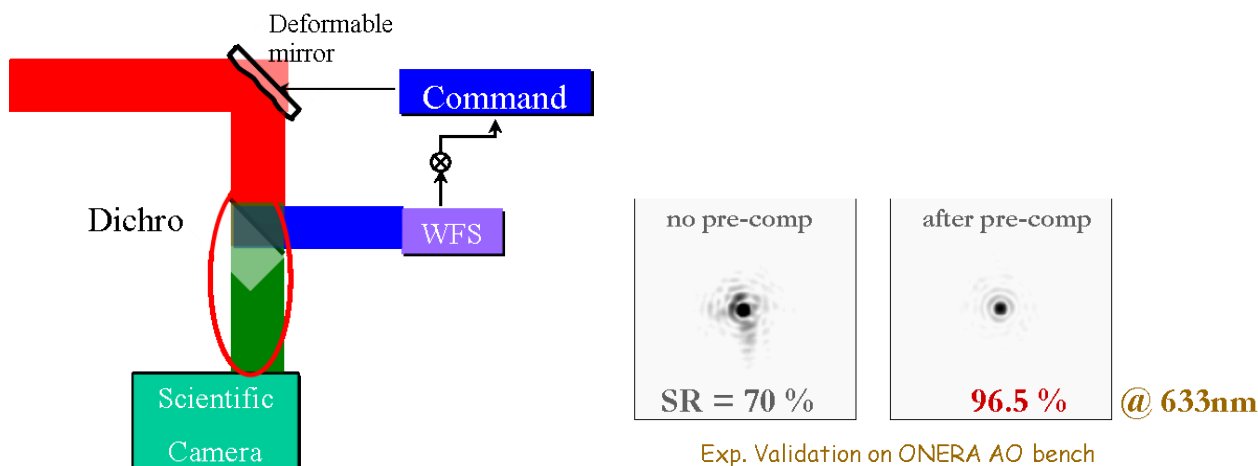


Figure 4. [Left] Principle of the NCPA pre-compensation using a phase diversity algorithm and the AO loop itself. [Right] Example of results obtained on the ONERA AO bench. The internal SR without pre-compensation is 70 % (@ 633 nm) and it goes up to 96.5 % after pre-compensation. 35 Zernike coefficients are corrected. This corresponds to less than 20 nm of global residual error and less than 3 nm on corrected modes.

7. AUXILIARY DEVICES

7.1. IR Tip-Tilt sensor

The average image position (in other words the optical axis position) on the coronagraphic mask is a main specification for the SPHERE system. The required accuracy for the mean image position is 0.5 mas or better. The global error for the average image position mainly depends on the differential refraction effect (between VIS and IR wavelengths) and the differential thermal or mechanical effects (between WFS and imaging paths). Considering the requirement, an open loop model of each differential evolution will not be accurate enough (considering all the possible parameters involved) to reach the absolute position performance. Therefore, to ensure that the specification will be fulfilled, an auxiliary IR tip-tilt sensor (AS) at the level of the coronagraphic mask has been proposed. This sensor will be coupled with a differential tip-tilt mirror (DTTM) located in an pupil plane in the WFS arms.

7.2. Pupil motion sensor

Pupil stability is a major issue to ensure the SPHERE performance. The pupil has to remain motionless during the whole observation process. When located after the Nasmyth focus of the telescope, this stability requirement implies a pupil de-rotator and a pupil re-centering device. It has been shown that a pupil shift of 1% of the pupil diameter or a pupil rotation of 1 degree will reduce by a factor of 1.5 to 2 (for typical conditions at the VLT) the detection capability of a coronagraphic + differential imaging system. This had led to impose a pupil stability in translation better than 0.2 (goal 0.1 %) of the full VLT pupil. This performance is achieved using a pupil tip-tilt mirror (PTTM) located close to the entrance focal plane of the SPHERE. This mirror is controlled

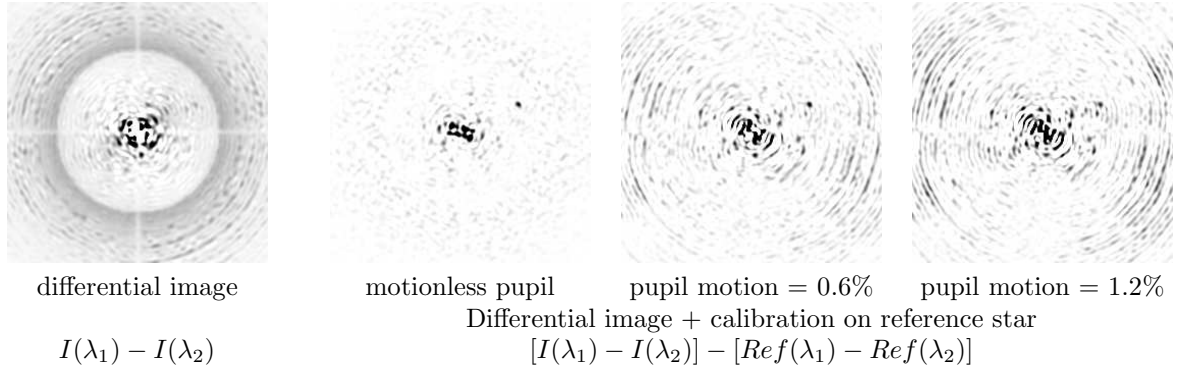


Figure 5. [Left] Differential coronagraphic (4-quadrant) image ($\lambda_1 = 1.56\mu m$, $\lambda_2 = 1.59\mu m$), [Right] differential coronagraphic image + reference subtraction: pupil shift between object and reference star = 0, 0.6 and 1.2 % of the full pupil. The companion ($\Delta_m = 15$, separation = 0.6 arcsec) is really distinguishable from residual fixed speckles for a fixed pupil.

by a pupil motion sensor (PMS). The PMS directly uses the SH-WFS data to measure pupil motion. Because pupil motion is rather slow, a measurement-correction process has to be performed typically every minute which ensures a good SNR on the PMS data.

8. GLOBAL SYSTEM DESIGN

As detailed before, the AO system for SPHERE, called SAXO (Sphere AO for eXoplanet Observation) is a challenging system composed by high performance sub-systems (high order DM, optimized RTC, EMCCD ...) A global trade-off from all the points mentioned above (combined with optical design, technological aspect, cost and risk issues) leads to the following AO system main characteristics:

- A 41x41 actuator DM of 180 mm diameter, located in a pupil plane with an inter-actuator stroke $> \pm 1\mu m$ (mechanical), a maximum stroke $> \pm 3.5\mu m$ (mechanical), plus a 2-axis TTM with a ± 0.5 mas resolution.
- 40x40 Shack-Hartmann WFS, with a spectral range between 0.45 and 0.95 μm , 6x6 pixels per sub-aperture (Shannon sampling @ 0.65 μm), a focal plane filtering device with variable size (from λ/d to $3\lambda/d$ at 0.7 μm) and a temporal sampling frequency 1kHz (goal 1.5 kHz). The foreseen detector is a 256x256 pixels Electron Multiplication CCD detector with a read-out-noise $< 1e^-$ and a 1.4 excess photon noise⁹
- Mixed numerical control law with a Kalman filter law for Tip-Tilt control and an Optimal Modal Gain Integrator law for DM control. The global AO loop delay (including CCD read-out and RTC delays) has to be lower than 1 ms (goal 666 μs)
- Non-common path aberrations: off-line measurements and on-line compensation using a phase diversity algorithm
- Auxiliary IR tip-tilt sensor and pupil sensor to measure and correct for optical axis and pupil displacement

The AO system gathers 3 closed loops as schematically described in Figure ??.

- the main AO loop (WFS-RTC-DM/TTM) working at 1.2 kHz
- the IR tip-tilt loop (Aux sensor-RTC-DTTM) working at 10-100 Hz for a fine centering of the optical axis on the coronagraph
- the pupil loop (SH intensities-RTC-PTTM) working at 0.1 Hz for a pupil stabilization.

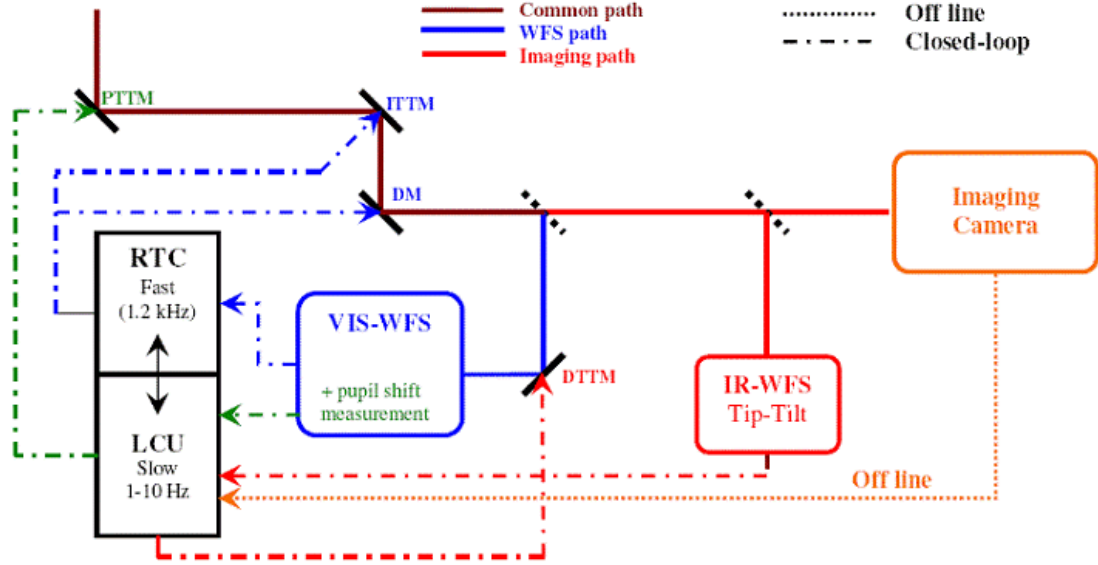


Figure 6. Schematic representation of the various loops in the AO system.

In addition, an off-line calibration (but on-line compensation) of the NCPA is also foreseen.

The realization phase of the SPHERE instrument has begun in March 2006. Optical and mechanical design are still in progress but the main choices have been done and first 3D scheme have been proposed for the implementation at the Nasmyth focus of the VLT (as shown in Figure 7).

Moreover, end-to-end simulations have been performed with this conceptual design. Results are summarized in Table 1. Using these AO simulations in a complete system model (including AO, coronagraphy, differential

Seeing conditions	0.65''		0.85		1.05''	
Spatial repartition	Low freq.	High freq.	Low freq.	High freq.	Low freq.	High freq.
Mag 9	46	51	54	67	67	81
Mag 11	64	51	73	67	90	81

Table 1. AO error budget (in nm rms) for various seeing and GS flux conditions. In each case, both low spatial frequency error (i.e corrected by AO) and high spatial frequencies error (fitting error) are given

imaging and detectivity process) it has been shown that these values satisfy the SPHERE high level requirements allowing direct detection of hot Jovian-like planets. An example of results is shown in Figure 8.

9. CONCLUSION

The AO system (SAXO) for SPHERE, the Planet Finder instrument on the VLT, represents a large step forward both in terms of system components and calibration procedures, nevertheless a complete analysis (with a detailed error budget) has shown that a AO system fulfilling all the requirement mandatory for the direct detection of hot Jupiter like planet is feasible in a reasonable time scale (5 years) with tried and tested technologies. After more than two years of preliminary studies, the main components of the AO system have been designed and the realization phase of the whole instrument has begun in March 2006 with an expected first light before the end of 2010.

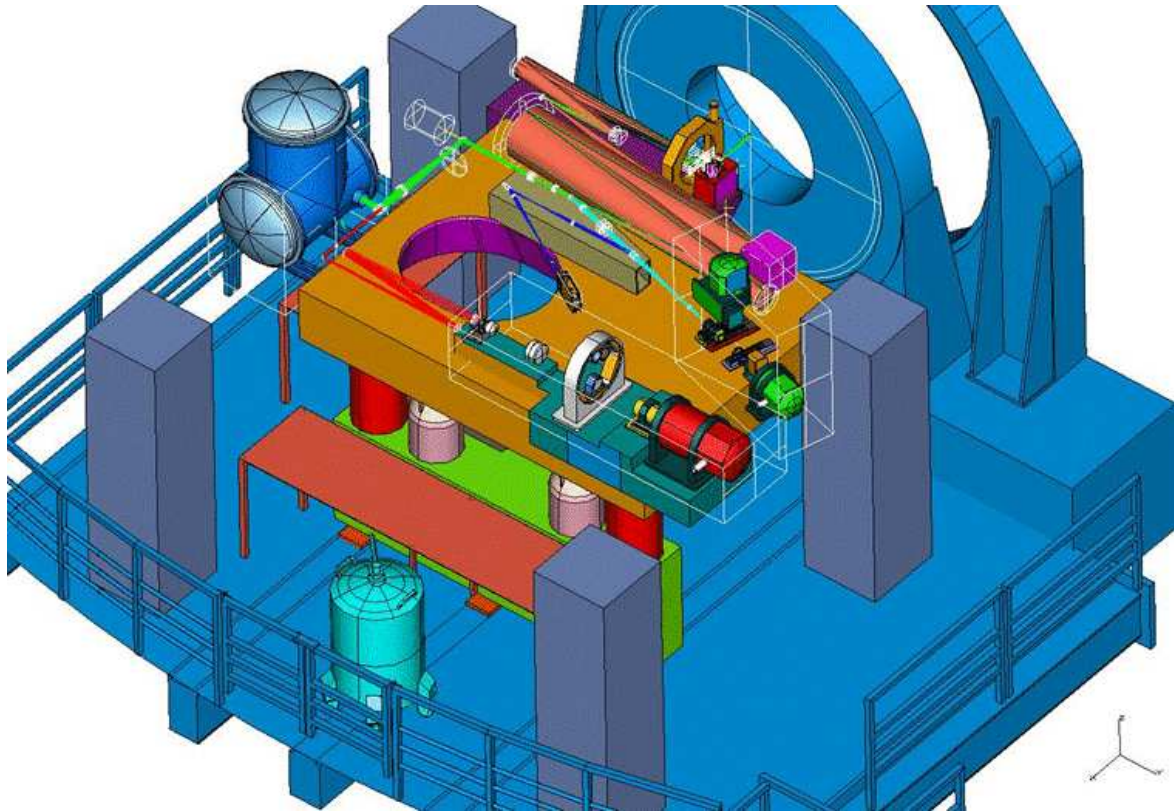


Figure 7. 3D view of the SPHERE system at Nasmyth focus of the VLT.

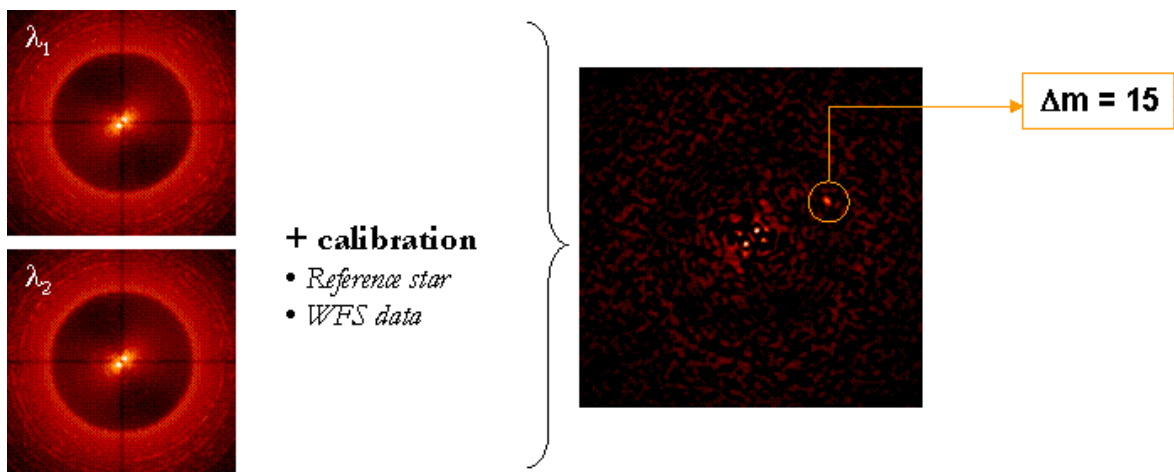


Figure 8. Example of simulation results. A planet with $\Delta_m = 15$ has been simulated and detected. Typical seeing conditions at Paranal and conservative assumptions on the system stability (pupil shift of 0.4 %, de-centering of 0.5 mas on the 4Q phase mask coronagraph, residual jitter of 3 mas rms, differential aberrations of 10 nm rms ...) have been considered. The GS magnitude is 8 in that simulation.

REFERENCES

1. J.-L. Beuzit, D. Mouillet, C. Moutou, K. Dohlen, P. Puget, T. Fusco, and A. e. a. Boccaletti, “A planet finder instrument for the vlt,” in *IAUC 200, Direct Imaging of Exoplanets: Science & Techniques*, 2005. Date conférence : Oct. 2005, Nice, France.
2. C. Moutou, J.-L. Beuzit, R. Gratton, and D. e. a. Mouillet, “A planet finder instrument for the vlt,” in *IAUC 200, Direct Imaging of Exoplanets: Science & Techniques*, 2006. Date conférence : Oct. 2005, Nice, France.
3. T. Fusco, G. Rousset, J.-F. Sauvage, C. Petit, J.-L. Beuzit, K. Dohlen, D. Mouillet, J. Charton, M. Nicolle, M. Kasper, and P. Puget, “High order adaptive optics requirements for direct detection of extra-solar planets. application to the sphere instrument.,” *Opt. Eng.* , accepted.
4. F. Roddier and C. Roddier, “Noao infrared adaptive optics program ii: modeling atmospheric effects in adaptive optics systems for astronomical telescopes,” in *Advanced Technology Optical Telescopes III*, L. D. Barr, ed., **628**, pp. 298–304, Proc. Soc. Photo-Opt. Instrum. Eng., Soc. Photo-Opt. Instrum. Eng., (Washington), 1986.
5. L. A. Poyneer and B. Macintosh, “Spatially filtered wave-front sensor for high-order adaptive optics,” *J. Opt. Soc. Am. A* **21**(5), pp. 810–819, 2004.
6. T. Fusco, C. Petit, G. Rousset, J.-M. Conan, and J.-L. Beuzit, “Closed-loop experimental validation of the spatially filtered Shack-Hartmann concept,” *Opt. Lett.* **30**, p. 1255, 2005.
7. C. Petit, F. Quiros-Pacheco, J.-M. Conan, C. Kulcsar, H.-F. Raynaud, T. Fusco, and G. Rousset, “Kalman filter based control loop for adaptive optics,” in *Advancements in Adaptive Optics*, **5490**, Proc. Soc. Photo-Opt. Instrum. Eng., SPIE, 2004. Date conférence : June 2004, Glasgow, UK.
8. M. Nicolle, T. Fusco, G. Rousset, and V. Michau, “Improvement of shack-hartmann wavefront sensor measurement for extreme adaptive optics,” *Opt. Lett.* **29**, pp. 2743–2745, Dec. 2004.
9. T. Fusco, M. Nicolle, G. Rousset, V. Michau, J.-L. Beuzit, and D. Mouillet, “Optimisation of Shack-Hartmann-based wavefront sensor for XAO system,” in *Advancements in Adaptive Optics*, **5490**, Proc. Soc. Photo-Opt. Instrum. Eng., 2004. Date conférence : June 2004, Glasgow, UK.
10. T. Fusco, G. Rousset, and A. Blanc, “Calibration of AO system. Application to NAOS-CONICA,” in *Science with Adaptive Optics*, W. Brandner and M. Kasper, eds., Springer-Verlag, 2004. Date conférence : Sept. 2003, Garching, Germany.
11. J.-F. Sauvage, T. Fusco, G. Rousset, and C. Petit, “Real-time and post-facto correction for differential aberrations in direct planet imaging by adaptive optics,” in *IAUC 200, Direct Imaging of Exoplanets: Science & Techniques*, 2005. Date conférence : Oct. 2005, Nice, France.